Sparse Recovery for Radar Applications

Alexander Ruthe (ayr2111)
ELEN-6867E Course Project S'2022

Electrical Engineering Department
Columbia University

New York, New York
ayr2111@columbia.edu

***Abstract*—Radar data is inherently sparse, with radar search sectors scanning wide fields of view for point targets and electronic strategy management (ESM) systems scanning the radiofrequency (RF) spectrum for narrowband and wideband activity to identify and track. This course project explores the exploitation of radar data sparsity in the dimensions of direction-of-arrival (DOA) and frequency with existing sub-Nyquist architectures and characterizes their performance across different configurations to determine when sub-Nyquist architectures are applicable.**

Keywords—sparsity, sub-Nyquist, direction-of-arrival, radar

I. Introduction

Search and detection in the radiofrequency (RF) spectrum are resource consuming processes for electronic management strategy (ESM) systems responsible for identifying and tracking RF activity. ESM systems have limited time with low-latency requirements, limited size and power with the modern push for edge-deployed systems, and limited digital bandwidths driven by analog-to-digital converter (ADC) sampling rate upper bounds. Fortunately, the search space dimensions of frequency and direction-of-arrival (DOA) are sparse, enabling use of sparse modeling and recovery to address these constraints while maintaining performance. This report explores the use of sparse recovery to search, detect, and reconstruct radar signals of interest and characterizes each method parametrically to outline their utility in different configurations. This report is outlined as follows: Section 2 outlines sparse recovery of radar signal frequency spectra and reconstruction results, Section 3 investigates sparse DOA estimation for expedited signal search, Section 4 introduces a combined approach for simultaneous angle-frequency recovery, and the paper is concluded with closing remarks in Section 5.

II. Spctrum Estimation

A. *Theory of Matrix Selection*

The restricted isometry property is defined by equation 1. It says that for a K_0-sparse signal $\boldsymbol{s}$ and a transformation matrix $\boldsymbol{A}$, sampling and reconstruction will succeed if δ is a small constant.

$$(1-\delta)\|\boldsymbol{s}\|_2^2 \leq \|\boldsymbol{A}\boldsymbol{s}\|_2^2 \leq (1+\delta)\|\boldsymbol{s}\|_2^2 \quad \forall 2K_0\text{-}\ sparse\ \boldsymbol{s} \quad (1)$$

The transformation matrix A defined by equation 2 is the product of a measurement matrix Phi and sparsity basis matrix Psi. The RIP is more likely to be met when Phi is incoherent with Psi, measured as the inner product of the matrices.

$$\boldsymbol{A} = \boldsymbol{\phi\Psi} \quad (2)$$

The frequency domain sparsity basis matrix can be several transforms including discrete Fourier transform (DFT), discrete cosine transform (DCT), and discrete wavelet transform (DWT). The measurement matrix is often designed as a pseudorandom bit sequence (a series of randomly selected +/-1) or gaussian random noise. The incoherence over a set of common measurement matrix codes and sparsity basis matrices and a simplified calculation of the RIP delta for the same set of transform matrices is summarized in Table 1. The number of measurements is ten, the number of frequency bins is 100, the sparse signal has five non-zero frequency components modeled as pure tones, and the DWT uses the Daubechies-4 wavelet. As expected, the delta values relative to the transform matrix are predicted by the incoherence for the same configurations. The results of Table 1 show that the maximum-length-sequence (MLS) and pseudorandom noise (PRN) sequence provide the best incoherence. Moreover, the Fourier-based and wavelet-based matrices outperform the cosine transform. Due to their relative implementation ease, the PRN measurement sequence with the DFT sparsity basis matrix is a good selection for most spectrum sensing applications.

B. *Sub-Nyquist Reconstruction of Radar Signals*

This section extends the Analog-to-Information-Converter (AIC) developed in [1] from the simple two-tone sinusoidal signal use case to a more realistic set of radar waveforms.

Technical Approach

This compressive sensing (CS) problem is formulated as acquiring an Nx1 sparse time domain signal $\boldsymbol{x}$ that is K-sparse in the sparsity basis matrix $\boldsymbol{\Psi}$, using an incoherent measurement matrix $\boldsymbol{\phi}$, based on the architecture in [1]. The formulation of results in the system equation:

$$\boldsymbol{y} = \boldsymbol{\phi x} = \boldsymbol{\phi\Psi z} \quad (3)$$

The signal x can be recovered from $M = Klog(N/K)$ linear projections onto a second basis Phi that is incoherent with the sparsity basis. As shown in Table 1, this condition is best met with a PRN measurement matrix and DWT or DFT sparse basis matrix. The recovery of the sparse set of coefficients is solved with a convex optimization procedure solving equation (3) for the l1-sparsest solution. The analog input signal to the system is given by:

$$x(t) = \sum_{n=1}^{N} \alpha_n \psi_n(t) \quad (4)$$

Table 1. Average Incoherence and R.I.P. Delta for Spectrum Compressive Sensing Matrices

Test Configuration		**CS Metrics**	
$\boldsymbol{\phi}$	$\boldsymbol{\Psi}$	*Incoherence*	*R.I.P. Delta*
MLS	DFT	0.496	529
Hadamard	DFT	1.000	1001
PRN	DFT	0.509	501
Gaussian	DFT	0.825	975
MLS	DCT	0.636	1534
Hadamard	DCT	1.282	2009
PRN	DCT	0.653	1640
Gaussian	DCT	1.058	1959
MLS	DWT	0.310	488
Hadamard	DWT	0.617	1001
PRN	DWT	0.309	497
Gaussian	DWT	0.507	951

where $\alpha_n\psi_n$ represents the sparse coefficients of the Fourier or Wavelet basis when there are a small number of nonzero entries in α_n. The signal is mixed with a higher-order frequency PRN sequence which spreads the frequency content of the signal to the lower part of the spectrum. Next, a low-pass filter (LPF) and sub-Nyquist analog-to-digital converter (ADC) reduce the signal to a low-rate measurement $\mathbf{y}$. The transform matrix can therefore be defined as:

$$\boldsymbol{V} = \boldsymbol{\phi\Psi} = \boldsymbol{\Psi P H} \tag{5}$$

Where P is the $M \times N$ PRN matrix, H is the diagonal LPF and downsampling matrix, and Psi is the sparse DFT matrix. The signal is then recovered via l1-optimiziation defined by

$$\hat{\boldsymbol{z}} = \arg min_z \|\boldsymbol{z}\|_1 \ \sigma.\tau. \ \boldsymbol{y} = \boldsymbol{\phi\Psi z} \tag{6}$$

The recovered and reconstructed waveform is correlated with the original signal and compared to the actual matched filter response to evaluate its utility. The peak-to-sidelobe ratio (PSLR) of the correlated reconstructed and original signals indicates how well the signals match. The main lobe level (MLL) side lobe level (SLL) are important metrics as well because not all mismatch losses are accounted for in the PSLR.

Experiments

The first experiment recovers a linear frequency modulated (LFM) radar waveform as shown in Figure 1. The pseudorandom noise bit sequence rate is 1 GHz, a factor of ten greater than the 100 MHz signal bandwidth. The analog input signal was modeled as having 2,000 discrete samples

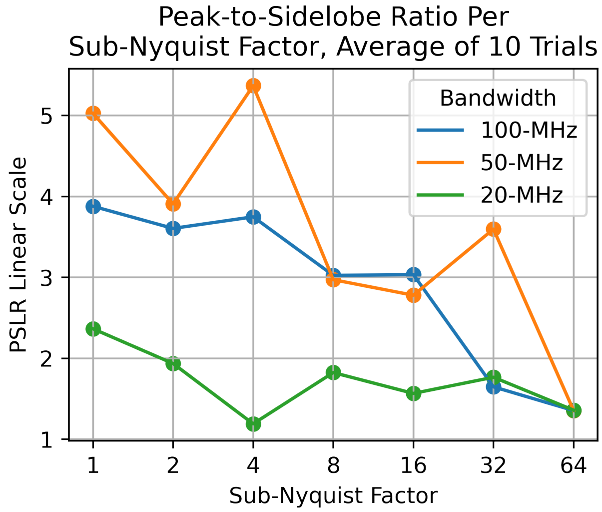

Figure 2: Peak-to-sidelobe ratio (PSLR) values of reconstructed signal match filtered with original signal across sub-Nyquist factors for different bandwidths.

over 200 ns. The anti-aliasing low pass filter (LPF) was set as one-half the ADC sample rate.

Sparse recovery was performed using the Least Absolute Shrinkage and Selection Operator (LASSO) package available in Scikit-Learn. The radar signal is reconstructed using an inverse fast Fourier transform (FFT) and compared to the original transmitted signal via matched filtering.

The results of Figure 1 show a reasonable ability to reconstruct the LFM signal for later use as a matched filter at a sub-Nyquist factor of eight. The ADC sample rate was adjusted over a range of sub-Nyquist factors and the subsequent recovery and reconstruction was evaluated by

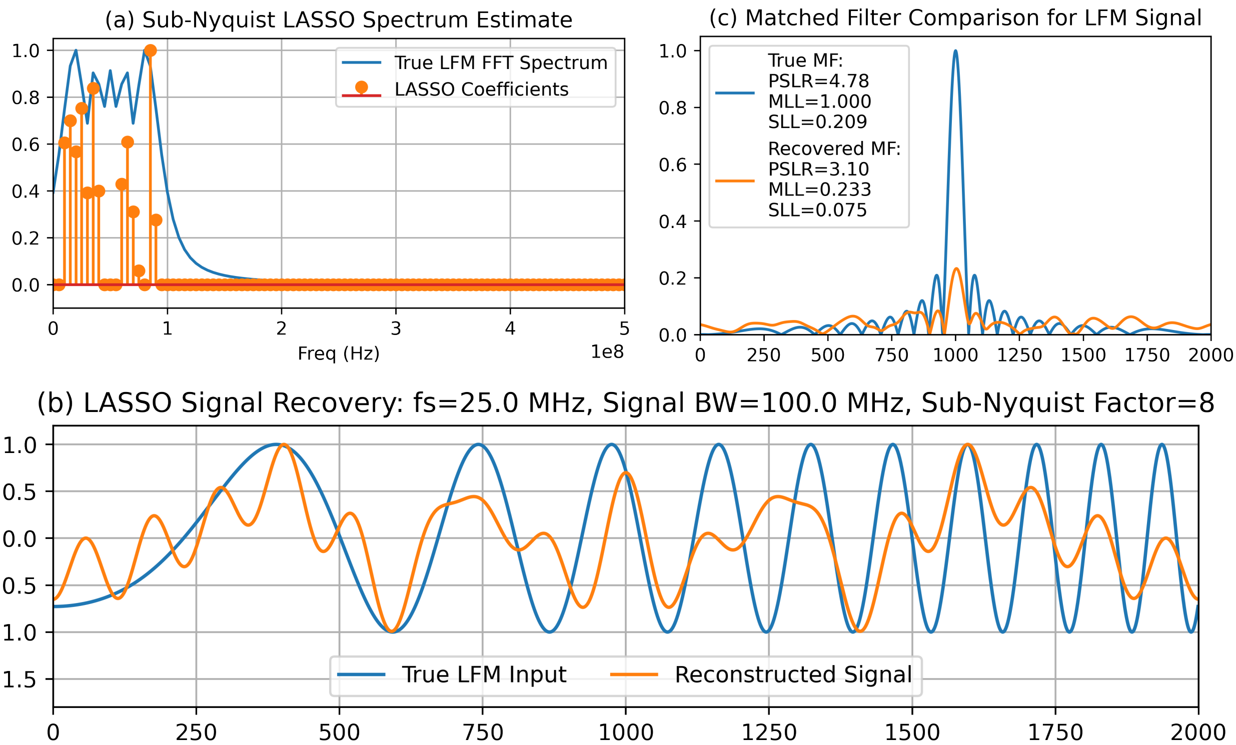

Figure 1: (a) LASSO recovered coefficients, (b) LFM signal reconstructed from coefficients, and (c) matched filter with original signal for LFM signal with 100-MHz bandwidth, subsampled in AIC architecture at 25MHz, equivalent to a sub-Nyquist factor of 8.

Table 2. LFM Sparse Signal Recovery and Reconstruction Matched Filter Characterization

Test Configuration		PSLR		MLL	SLL
BW (MHz)	*Sub-Nyquist*	*Mean*	*Variance*	*Mean*	*Mean*
100	64	1.355	0.134	0.111	0.084
100	32	1.648	0.726	0.075	0.058
100	16	3.034	0.370	0.116	0.040
100	8	3.025	0.554	0.158	0.055
100	4	3.748	0.669	0.308	0.086
100	2	3.605	1.383	0.306	0.092
100	1	3.878	2.514	0.311	0.090
50	64	1.356	0.353	0.152	0.115
50	32	3.596	12.373	0.123	0.067
50	16	2.779	0.930	0.070	0.031
50	8	2.971	3.423	0.104	0.053
50	4	5.367	11.646	0.186	0.047
50	2	3.907	4.811	0.260	0.083
50	1	5.026	11.936	0.134	0.035
20	64	1.360	0.277	0.109	0.090
20	32	1.766	1.506	0.231	0.152
20	16	1.566	0.416	0.056	0.042
20	8	1.824	0.602	0.152	0.101
20	4	1.191	0.142	0.091	0.082
20	2	1.936	1.277	0.058	0.039
20	1	2.365	2.929	0.118	0.071

measured in terms of PSLR as shown in Figure 2. Multiple bandwidths are shown as a proxy for sparsity. Moreover, the LASSO lambda values that weight the l1-norm relative to the l2-loss in the objective function is shown to describe how the relationship scales with the sub-Nyquist factor. These values are summarized across test configurations in Table 2.

In addition to the LFM, a multiple phased-shift-keyed (MPSK) signal is simulated, recovered, and reconstructed using the AIC framework with results shown in Figure 3. The signal is recovered at a sub-Nyquist factor of 2, meaning the sample rate equals the bandwidth. While the matched filter analysis is less useful for this type of signal, the recovered support and reconstructed time domain signal closely approximate the original. This indicates that a sub-Nyquist sampling architecture like this could be used for low-rate communications in low size-weight-and-power (SWaP) edge devices working within a network of higher data rate devices.

III. Phased Array DOA Estimation

This section explores direction of arrival (DOA) estimation for a uniform linear array and characterizes the performance across key metrics based on [2].

Technical Approach

An N-element uniform linear array receives RF signals from various DOA's according to the steering vector of the array **a**, narrowband signal **s**, and additive noise **w** given by:

$$\boldsymbol{x}(t) = \sum_{k=1}^{K} \boldsymbol{a}(\theta_k) s_k(t) + \boldsymbol{w}(t) \tag{7}$$

where the steering vector corresponding to the N-element uniform linear array is:

$$\boldsymbol{a}(\theta) = \left[1\ e^{-j\alpha} \ldots\ e^{-j\alpha(N-1)}\right] \tag{8}$$

where $\alpha = 2\pi\left(\frac{d}{\lambda}\right)\sin(\theta)$ is the phase shift across array elements based on element spacing d, and wavelength λ. The received signal vector can be arranged in a format suitable for sparse recovery as:

$$\boldsymbol{x}(t) = \boldsymbol{A}\boldsymbol{s}(t) + \boldsymbol{w}(t) \tag{9}$$

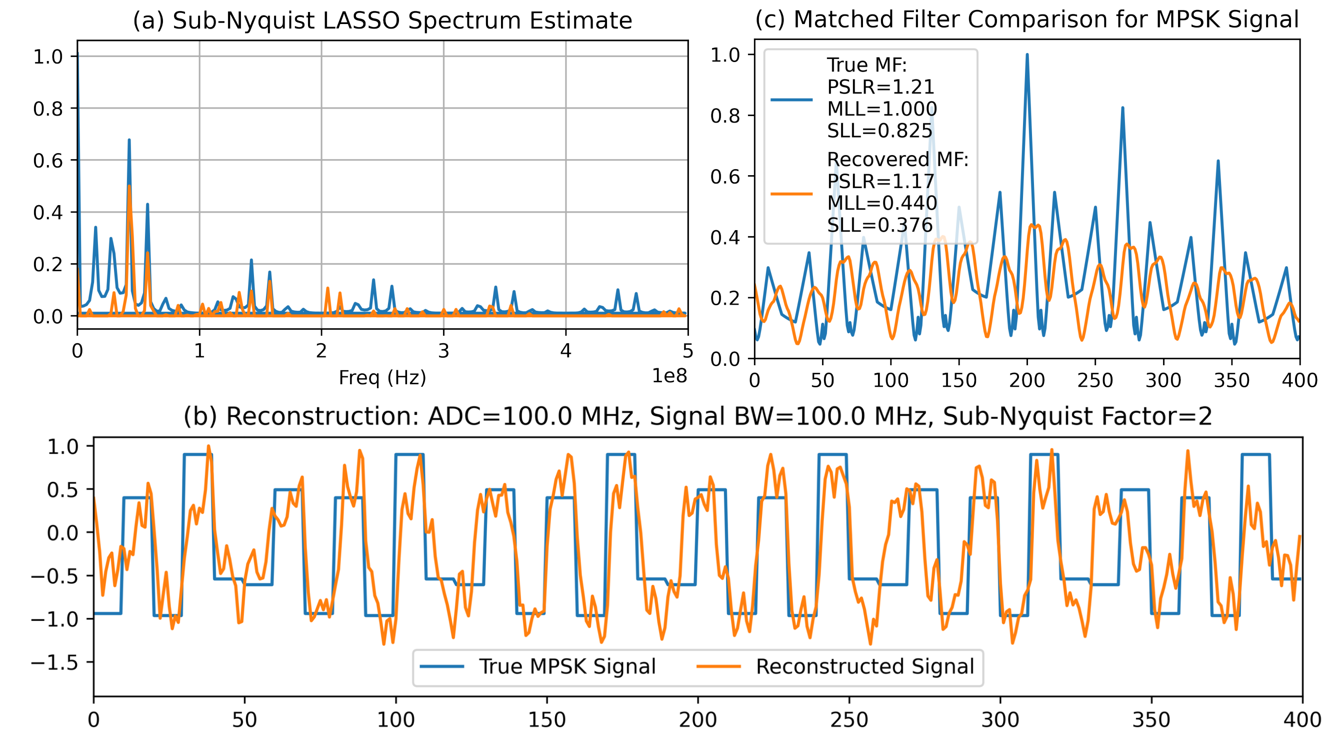

Figure 3: (a) LASSO recovered coefficients, (b) MPSK signal reconstructed from coefficients, and (c) matched filter with original signal for 100-MHz-BW MPSK signal, subsampled in AIC architecture at 100 MHz, a sub-Nyquist factor of 2.

where A is the $N \times K$ matrix form of (8) with each column representing a different angle in the search space and s(t) is the Kx1 source vector. The formulation of (9) can be leveraged in a compressive sensing architecture:

$$\boldsymbol{y} = \boldsymbol{\phi x} = \boldsymbol{\phi \Psi z} \qquad (10)$$

where $\boldsymbol{\phi}$ is the measurement matrix, $\boldsymbol{\Psi}$ is the sparse basis matrix, x is the received signal, $\boldsymbol{y}$ is the measurement vector, and $\boldsymbol{z}$ is the desired sparse vector representing the DOAs being solved for. The compressive sensing architecture is taken from [2] where **M** random measurement sequences in $\boldsymbol{\phi}$ are taken across **N** array elements. The sparse basis matrix $\boldsymbol{\Psi}$ is the steering response vector of the uniform linear array over the $N_s$scan angles given by:

$$\boldsymbol{\Psi} = [\boldsymbol{a}(\theta_1)\ \boldsymbol{a}(\theta_2) \ldots \boldsymbol{a}(\theta_{N_s})] \qquad (11)$$

Thus, **z** is the recovered sparse angle spectrum vector with $N_s$entries given by:

$$\boldsymbol{z} = \left[\boldsymbol{z}_{\theta_1}\ \boldsymbol{z}_{\theta_2} \ldots \boldsymbol{z}_{\theta_{N_s}}\right] \qquad (12)$$

Which can be recovered following the l1-norm optimization problem:

$$\hat{\boldsymbol{z}} = \arg min_z \|\boldsymbol{z}\|_1 \ \sigma.\tau.\ \boldsymbol{y} = \boldsymbol{\phi \Psi z} \qquad (13)$$

Experiments

The simulated uniform linear array has N = 64 elements. The number of sources K = 2, with multiple phase shift keying (MPSK) modulation. The signal-to-noise ratio (SNR) is 20 dB and the true DOA's are 0 and 15 degrees with respect to array boresight. The number of time snapshots is **T=1** in contrast to T=60 used in [2] because all information needed for DOA estimation is in one time sample. The number of scan angles N_s is 181 for an angle resolution of 1 degree for a search space [-90, 90]. The measurement matrix $\boldsymbol{\phi}$ is a pseudorandom bit sequence in {-1,1}, and the number of

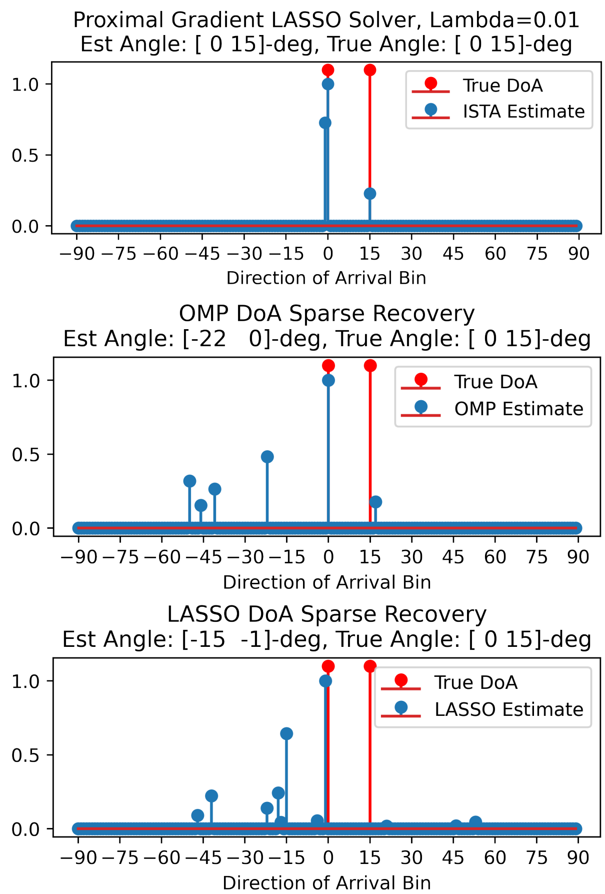

Figure 4: DoA sparse recovery of a two-source simulation for (top) Proximal Gradient LASSO, (middle) OMP, and (bottom) LASSO.

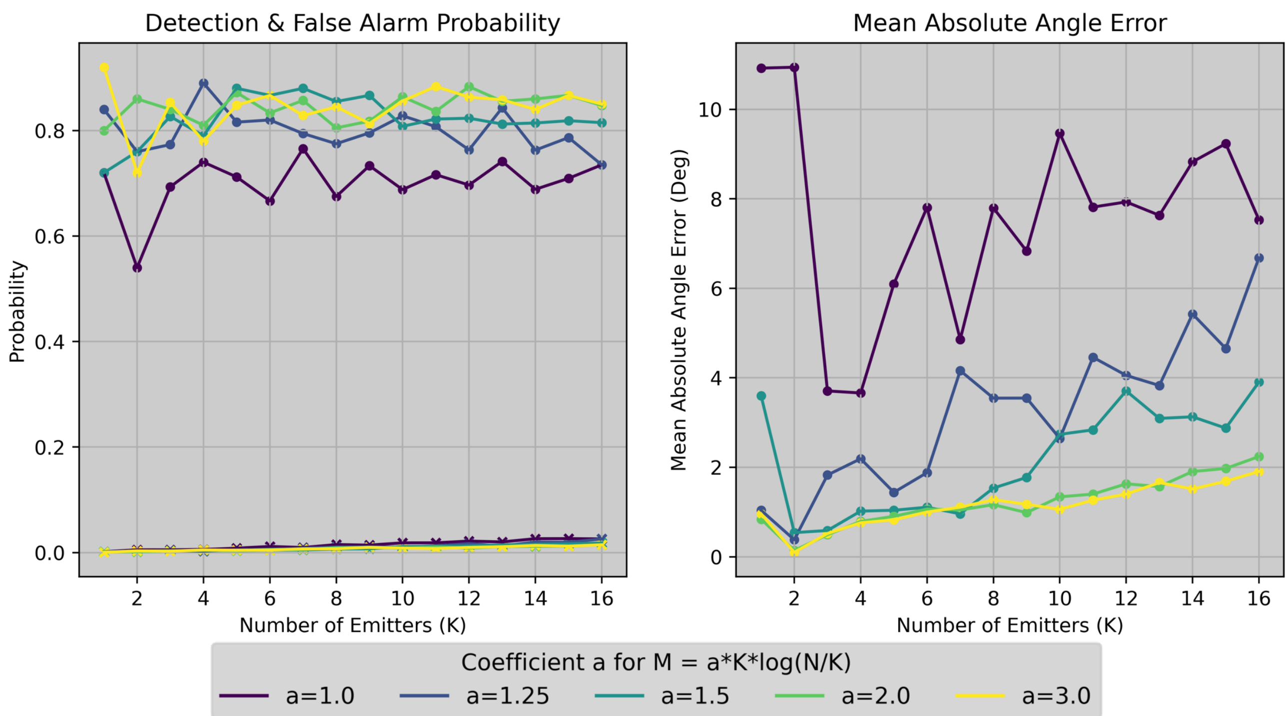

Figure 5: DOA accuracy results for different measurement branch values averaged across 25 trials.

Table 3. DOA CS Architecture Characterization

Test Configuration				Angle Estimates		
N	K	$\Delta\theta$	*Mod Type*	*Angle Error*	*PD*	*PFA*
64	1	0.0	MPSK	0.880	0.840	0.001
32	1	0.0	MPSK	0.880	0.840	0.001
16	1	0.0	MPSK	26.480	0.600	0.002
8	1	0.0	MPSK	68.880	0.040	0.005
64	2	1.0	MPSK	0.500	0.840	0.002
64	2	5.0	MPSK	3.920	0.840	0.002
64	2	10.0	MPSK	1.900	0.660	0.004
64	2	15.0	MPSK	2.180	0.740	0.003
64	2	30.0	MPSK	4.880	0.760	0.003
64	2	45.0	MPSK	3.220	0.900	0.001
64	2	1.0	LFM	2.160	0.660	0.004
64	2	1.0	MPSK	1.440	0.720	0.003
64	2	5.0	LFM	0.980	0.820	0.002
64	2	5.0	MPSK	1.780	0.820	0.002
64	2	10.0	MPSK	4.480	0.760	0.003
64	3	10.0	MPSK	10.360	0.587	0.007
64	4	10.0	MPSK	12.860	0.550	0.010
64	5	10.0	MPSK	23.264	0.304	0.020
64	6	10.0	MPSK	20.840	0.333	0.023
64	2	15.0	MPSK	5.360	0.740	0.003
64	3	10.0	MPSK	16.147	0.613	0.007
64	4	7.5	MPSK	14.720	0.500	0.011
64	5	6.0	MPSK	19.856	0.384	0.018
64	6	5.0	MPSK	22.300	0.380	0.021

measurement branches M=10. The CS recovery algorithms implementations used include proximal gradient least absolute shrinkage and selection operator (LASSO) [3], orthogonal matching pursuit (OMP) [4], and LASSO [4].

The results across CS algorithms are shown in Figure 4. Proximal gradient LASSO recovery generally performed better than the other methods. OMP frequently recovered smaller support vectors near the correct DOAs but had larger erroneous support estimates masking those. LASSO often estimated the negative of the true DOA as seen in Figure 4, which is likely caused by the steering vectors at positive-negative angle pairs being mirrored copies of each other.

The key configurations of the DOA CS architecture were characterized and summarized in Table 3. Reducing the number of array elements and increasing the cardinality reduce DOA angle estimation accuracy. However, reducing the target spacing or changing the waveform has minimal impact on the accuracy.

The number of hardware branches M is expected to impact the recovery accuracy most significantly. To measure this, the CS architecture is characterized across probability of detection, false alarm probability, and mean absolute angle error for different values of M. Specifically, the number of measurement branches is adjusted through coefficient a in $M = aK\log(N/K)$ where the theoretical minimum number of measurements for recovery is when $a = 1$. In this case, K is the number of emitters and N is the number of scan angles N_s. The result of this analysis is shown in Figure 5. The angle error and probability of detection appear to reach a stable solution for $m \geq 2$ with minimal angle and detection probability errors. The theoretical minimum number of measurements when $a = 1$ shows considerable error, which could be due to non-zero coherence between the sparse matrix and measurement matrix.

IV. Joint Frequency-Angle Estimation

Towards the goal of simultaneous angle and frequency sparse support recovery from phased array I/Q data, [5] leverages a 2D architecture based on the sparse basis matrix:

$$\boldsymbol{\Psi}_{freq-angle} = (\boldsymbol{I}_M \otimes \boldsymbol{W}_N^H)\boldsymbol{P} \tag{14}$$

Where $\boldsymbol{I}_M$ is the identity matrix for an M-element array, $\boldsymbol{W}_N^H$ is the inverse discrete Fourier transform matrix, and $\boldsymbol{P}$ is a permutation matrix that arranges columns so vectors with the same frequency are contiguous. A scenario with three emitters at angles 56.25, 11.25, 33.75 degrees and 100, 200, 350 MHz respectively all with MPSK modulations at 20 dB SNR is simulated. The number of time samples is 250, the number of antenna elements is 4, the measurement matrix is a PRN matrix, and recovery is performed with OMP. The results shown in Figure 6 don't converge to the true result.

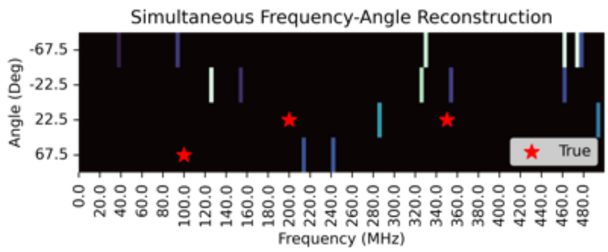

Figure 6: Angle-frequency sparse recovery of three-source simulation using OMP and sparse basis matrix from (14).

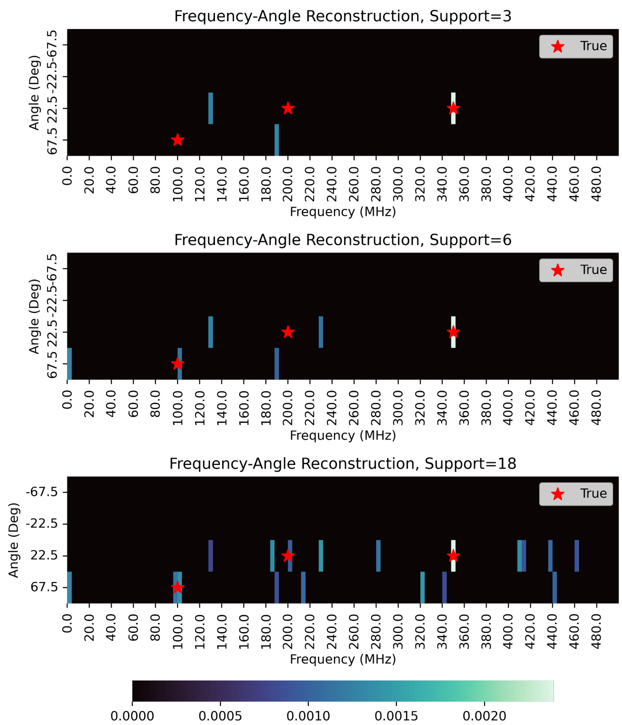

Figure 7: Angle-frequency sparse recovery of three-source simulation using OMP and sparse basis matrix from (15) across three different configurations for number of OMP supports recovered, 3, 6, and 18.

A second sparse basis matrix based on the DFT and beamsteering matrices shown previously and is given as:

$$\boldsymbol{\Psi}_{\boldsymbol{freq-angle}} = \boldsymbol{D}_{\boldsymbol{n_s}} \otimes \boldsymbol{B}_{\boldsymbol{N}} \tag{15}$$

where $\boldsymbol{D}_{\boldsymbol{n_s}}$ is the DFT matrix for $\boldsymbol{n_s}$ time samples and $\boldsymbol{B}_{\boldsymbol{N}}$ is the beamsteering matrix defined in (11) for an $\boldsymbol{N}$-element array. The same scenario and configuration are used to test (15), initially under the condition of Nyquist-rate sampling. Those results are shown in Figure 7, which shows that for K=3, the true number of emitters, the algorithm can correctly recover one emitter's angle-frequency support with the largest support vector. Increasing the number of OMP supports to 6, yields an improved result with two emitters correctly identified by the algorithm. The number of supports has to be increased to 18 in order to achieve a result where all three emitters are accounted for in the recovered support.

With some confidence that this method is feasible, subsampling was introduced to the above scenario at half Nyquist-rate. These results are shown in Figure 8 for the same number of supports as above. The recovery algorithm is unable to recovery any of the supports in all configurations.

V. Conclusions

This report has shown that common radar signals can be reasonably recovered at large sub-Nyquist factors and reconstructed using l_1 -optimization methods in one dimension for frequency and angle dimensions. Additionally, it was shown that uniform linear arrays can estimate K DOA's using $M = 2Klog(N/K)$ or more measurements to achieve a PD of approximately 0.85 and a mean absolute angle error less than 2 degrees for radar waveforms. Combining the one-dimensional sparse recovery methods into a two-dimensional joint angle-frequency recovery method was investigated following one of the only references on the matter as well as a naïve approach combining the one-dimensional methods. In both cases, sub-Nyquist rate join recovery was not achieved, but in the latter case combining the beamsteering and Fourier sparse bases with the Kronecker product, preliminary results at Nyquist rate showed that the joint support recovery is at least feasible.

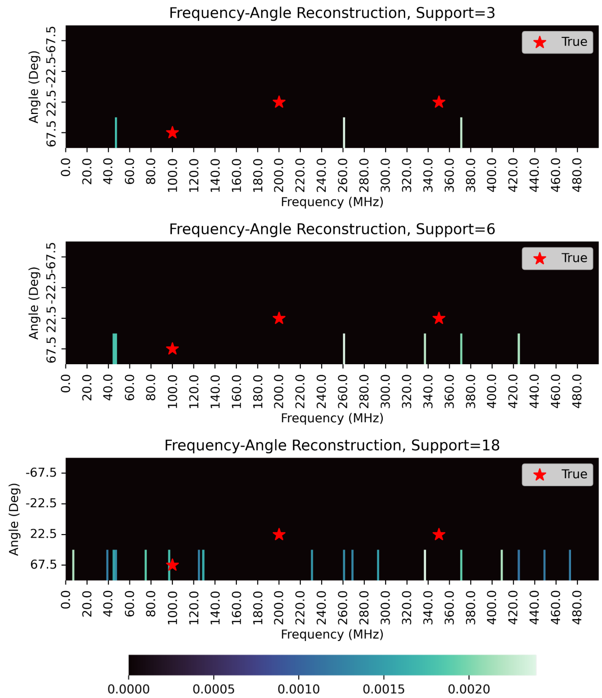

Figure 8: Angle-frequency sparse recovery of three-source simulation using OMP and sparse basis matrix from (15) with a sub-Nyquist factor of two.

References

[1] S. Kirolos *et al.*, "Analog-to-Information Conversion via Random Demodulation," *2006 IEEE Dallas/CAS Workshop on Design, Applications, Integration and Software*, 2006, pp. 71-74, doi: 10.1109/DCAS.2006.321036

[2] Ying Wang, G. Leus and A. Pandharipande, "Direction estimation using compressive sampling array processing," *2009 IEEE/SP 15th Workshop on Statistical Signal Processing*, 2009, pp. 626-629, doi: 10.1109/SSP.2009.5278497

[3] Wright, J. (2022) Proximal Gradient LASSO Algorithm. [Class Material].

[4] Scikit-learn: Machine Learning in Python, Pedregosa *et al.*, JMLR 12, pp. 2825-2830, 2011.

[5] B. Miller, J. Goodman and K. Forsythe, "Compressed Sensing Arrays for Frequency-Sparse Signal Detection and Geolocation," *2009 DoD High Performance Computing Modernization Program Users Group Conference*, 2009, pp. 297-301, doi: 10.1109/HPCMP-UGC.2009.48.